Biophysical Chemistry, 36 (1990) 99–115
Elsevier

BIOCHE 01436

Conformational distributions of melittin in water / methanol mixtures from frequency-domain measurements of nonradiative energy transfer

Joseph R. Lakowicz [a], Ignacy Gryczynski [a], Wieslaw Wiczk [a], Gabor Laczko [a], Franklyn C. Prendergast [b] and Michael L. Johnson [c]

[a] *University of Maryland School of Medicine, Department of Biological Chemistry, 660 West Redwood Street, Baltimore, MD 21201,* [b] *Mayo Foundation, Department of Biochemistry & Molecular Biology, 200 First Street, S.W., Rochester, MN 55905* *and* [c] *University of Virginia, Department of Pharmacology, Charlottesville, VA 22908, U.S.A.*

Received 17 November 1989
Revised manuscript received 4 December 1989
Accepted 4 December 1989

Fluorescence spectroscopy; Energy transfer; Time-resolved fluorescence; Frequency-domain fluorescence; Melittin; Distance distribution

We used fluorescence energy transfer to examine the effects of solvent composition on the distribution of distances between the single tryptophan residue of melittin (residue 19) to the N-terminal α-amino group, which was labeled with a dansyl residue. The tryptophan intensity decays, with and without the dansyl acceptor, were measured by the frequency-domain method. The data were analyzed by a least-squares algorithm which accounts for correlation between the parameters. A wide distribution of tryptophan to dansyl distances was found for the random-coil state, with a Gaussian half-width of 25 Å. Increasing concentrations of methanol, which were shown to induce an α-helical conformation, resulted in a progressive decrease in the width of the distribution, reaching a limiting half-width of 3 Å at 80% (v/v) methanol. The distance from the indole moiety of Trp-19 to the dansyl group in 80% (v/v) methanol/water was found to be 25 Å, as assessed from the center of the distance distribution. A distance of 24–25 Å was recovered from the X-ray crystal structure of the tetramer, which is largely α-helical. At low ionic strength (< 0.01) the CD spectra revealed a small fraction or amount of α-helix for melittin in water, which implies a small fraction of residual structure. This residual structure is apparently lost in guanidine hydrochloride as demonstrated by a further broadening in the distribution of distances. These results demonstrate the usefulness of frequency-domain measurements of resonance transfer for resolution of conformational distributions of proteins.

1. Introduction

Nonradiative or resonance energy transfer (RET) has been widely used to measure the dimensions of biological macromolecules [1–3]. The high sensitivity of fluorescence methods allows measurements on dilute solutions of protein, and the characteristic distance for fluorescence resonance energy (FRET) transfer (Förster distance, R_0) is typically near 30 Å [4], a value comparable to the diameters of many soluble proteins. In general, resonance energy transfer has been applied to systems where a single conformational state is expected, for example, in the study of globular proteins in their native (folded) conformation. However, it is apparent from first principles that a single or a static distance is unlikely to occur, particularly if the peptide chain can adopt

Correspondence address: J.R. Lakowicz, University of Maryland, School of Medicine, Department of Biological Chemistry, 660 West Redwood Street, Baltimore, MD 21201, U.S.A.
Abbreviations: Ac, acrylamide; dansyl, 1-dimethylamino-5-sulfonylnaphthalene; CD, circular dichroism; Gdn · HCl, guanidine hydrochloride; Mops, 3-(*N*-morpholino)propanesulfonic acid; MeOH, methanol; RET, resonance energy transfer.

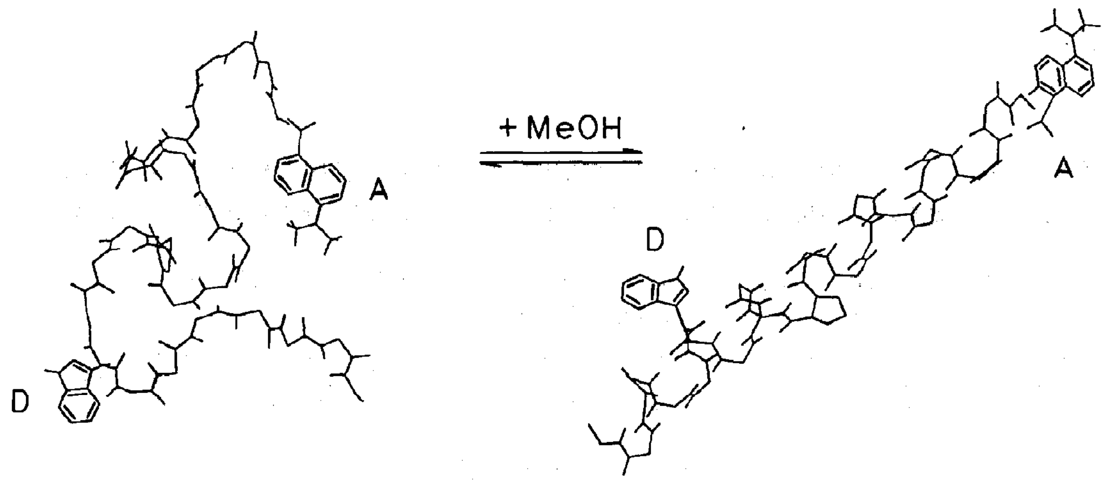

Scheme 1. Random-coil and α-helical melittin.

various conformations or if there are substantial segmental motions occurring on the same time scale as the fluorescence emission. Such motions or conformational variability should give rise to a distribution of distances, which in turn should be recoverable from the intensity decays of the donor in an energy-transfer experiment.

In the present article, we describe an extension of the FRET measurements to recover the distribution of distances between two sites on a protein which can adopt a variety of conformations. More specifically, we measured energy transfer from the single tryptophan residue of melittin (donor, D) to a dansyl (acceptor, A) located specifically on the α-amino group of the N-terminal lysine. The conformation of melittin was varied from the presumably random coil state in water (low ionic strength) to the α-helical form in 80% methanol (scheme 1). Under these varied conditions, we examined the intensity decays of the tryptophan residue using the frequency-domain method [4–7]. A distribution of D to A distances results in a distribution of rate constants for energy transfer, which alter the frequency response of the tryptophan emission. The distance distributions are recovered by a non-linear least-squares method which compares the frequency response of the donor emission, with and without the acceptor [8–10]. To confirm further the recovered distributions and to improve the resolution, we also performed a global analysis of data obtained at various R_0 values, which were obtained using collisional quenching of the tryptophan donor [11,12]. Finally, the distances were compared to that expected for melittin in the random-coil and α-helical states, the latter being found from the known X-ray structure of melittin [13].

It should be noted that this type of measurement is an extension of the pioneering work of Haas, Steinberg and co-workers. These researchers used time-domain fluorescence methods to examine end-to-end distributions of peptides [14,15], including the estimation of end-to-end diffusion coefficients [16,17].

2. Theory

2.1. Single exponential donor decays

The theory of energy transfer in the presence of a distance distribution is complex. To simplify the presentation, we first describe the simpler case where the donor decay, in the absence of acceptor or collisional quenching, is a single exponential. Assume the decay of the donor ($I_D(t)$), in the absence of energy transfer or quenching, is a single exponential

$$I_D(t) = I_D^0 \exp[-t/\tau_D^0] \tag{1}$$

where τ_D^0 denotes the decay time of the donor (D). The superscript (0) indicates the absence of quencher (Q). If a single acceptor is present in a unique distance r, then donor decay is given by

$$I_{DA}(r,t) = I_D^0 \exp[-t/\tau_D^0 - k_{DA}t]. \tag{2}$$

The rate of energy transfer is given by

$$k_{DA} = \frac{1}{\tau_D^0}\left(\frac{R_0}{r}\right)^6 \tag{3}$$

with R_0 being the Förster distance. For the case of a single acceptor at a unique distance, the donor decay remains a single exponential and the decay time is given by

$$\frac{1}{\tau_{DA}} = \frac{1}{\tau_D^0} + k_{DA}. \tag{4}$$

The Förster distance R_0 can be calculated from the spectral properties of the chromophores [4],

$$R_0^6 = \frac{9000(\ln 10)\kappa^2\phi_D^0}{128\pi^5 N n^4}\int_0^\infty F_D(\lambda)\epsilon_A(\lambda)\lambda^4\,d\lambda \tag{5}$$

where κ^2 is the orientation factor, ϕ_D^0 the quantum yield of the donor in the absence of acceptor and quencher, n the refractive index, and N Avogadro's number; $F_D(\lambda)$ describes the emission spectrum of the donor with the area normalized to unity, $\epsilon_A(\lambda)$ is the absorption spectrum of the acceptor in units of M^{-1} cm^{-1}, and λ is the wavelength in nm. The distances recovered from energy-transfer measurements are uncertain due to the unknown extent of static and dynamic averaging of the orientation factor [18]. In our analysis we assume the value of κ^2 is equal to 2/3 due to the range of conformations, the possibility of rotational diffusion, and the mixed polarization of the species [19].

The intensity decay of the donor becomes more complex if the acceptor is located over a range of D-A distances, as is expected for a random-coil protein. Since each individual D-A pair is characterized by a specific distance r, the intensity decay of each donor molecule is still a single exponential and is given by

$$I(r,t) = k \exp\left[-\frac{t}{\tau_D^0} - \frac{t}{\tau_D^0}\left(\frac{R_0}{r}\right)^6\right]. \tag{6}$$

However, the observed decay contains contributions from D-A pairs at all accessible distances, and is thus more complex than a single exponential. The intensity decay of the ensemble of D-A pairs is given by the average of the individual decays weighted by the distance probability distribution ($P(r)$) of the D-A pairs [14,16].

$$I_{DA}(t) = I_D\int_0^\infty P(r) \exp\left[-\frac{t}{\tau_D^0} - \frac{t}{\tau_D^0}\left(\frac{R_0}{r}\right)^6\right] dr. \tag{7}$$

This expression is appropriate for a distribution in which the D-A distances are static during the donor decay, which we assumed to be the case in our measurements.

To characterize the distance distributions and to minimize the number of variable parameters we assumed that the distribution is adequately described by a Gaussian,

$$P(r) = \frac{1}{\sigma\sqrt{2\pi}} \exp\left[-\frac{1}{2}\left(\frac{r-\bar{r}}{\sigma}\right)^2\right] \tag{8}$$

where $\bar{r}$ is the average and σ the standard deviation of the distribution. The standard deviation is related to the half-width, hw (full-width at half-maximum) by hw = 2.354σ.

2.2. Frequency-domain expressions

The intensity decays of the donor emission were measured using the frequency-domain method. The experimental values are the phase (ϕ_ω) and modulation (m_ω) of the emission over a range of modulation frequencies (ω). Irrespective of the form of the decay the frequency-response can be predicted for any $I(t)$ using

$$N_\omega = \frac{\int_0^\infty I(t) \sin \omega t\, dt}{\int_0^\infty I(t)\, dt} \tag{9}$$

$$D_\omega = \frac{\int_0^\infty I(t)\cos\omega t\,\mathrm{d}t}{\int_0^\infty I(t)\,\mathrm{d}t} \tag{10}$$

The calculated (c) phase and modulation values for the assumed decay law are given by

$$\phi_{c\omega} = \arctan\left[\frac{N_\omega}{D_\omega}\right] \tag{11}$$

$$m_{c\omega} = \left[N_\omega^2 + D_\omega^2\right]^{1/2} \tag{12}$$

The frequency-domain donor decays were routinely analyzed using the multiexponential model, which reveals the mean decay time of the decay and the extent of decay time heterogeneity. In this case $I(t)$ is given by

$$I(t) = \sum_i \alpha_i \exp[-t/\tau_i] \tag{13}$$

where α_i are the pre-exponential factors and τ_i the associated decay times. The transforms of eqs 9 and 10 can be represented analytically [20]

$$N_\omega = \frac{1}{J}\sum_i \frac{\alpha_i\omega\tau_i^2}{1+\omega^2\tau_i^2} \tag{14}$$

$$D_\omega = \frac{1}{J}\sum_i \frac{\alpha_i\tau_i}{1+\omega^2\tau_i^2} \tag{15}$$

where the normalization factor is given by $J = \sum_i \alpha_i\tau_i$. For a distribution of D-A distances the transforms are calculated numerically, using

$$N_\omega = \frac{1}{J}\int_{r=0}^\infty \frac{P(r)\omega\tau_{DA}^2}{1+\omega^2\tau_{DA}^2}\mathrm{d}r \tag{16}$$

$$D_\omega = \frac{1}{J}\int_{r=0}^\infty \frac{P(r)\tau_{DA}}{1+\omega^2\tau_{DA}^2}\,\mathrm{d}r \tag{17}$$

where the normalization factor J is given by

$$J = \left(\int_0^\infty P(r)\,\mathrm{d}r\right)\left(\int_0^\infty I_{DA}(t)\,\mathrm{d}t\right) \tag{18}$$

Depending upon $P(r)$, the integral from $r=0$ to ∞ may not be equal to unity. This integral will be less than unity when part of the distribution occurs below $r=0$. The use of $\int_0^\infty P(r)$ in eq. 18 is equivalent to normalizing $P(r)$ to unity. It should be borne in mind that eqs. 16 and 17 contain τ_{DA}, which is itself dependent upon the D-A distance (eq. 4).

The parameters describing the intensity decay (α_i and τ_i or $\bar{r}$ and σ) are determined using nonlinear least squares [21]. The parameter values are estimated by minimizing χ_R^2,

$$\chi_R^2 = \frac{1}{\nu}\sum_\omega\left[\frac{\phi_\omega-\phi_{c\omega}}{\delta\phi}\right]^2 + \frac{1}{\nu}\sum_\omega\left[\frac{m_\omega-m_{c\omega}}{\delta m}\right]^2 \tag{19}$$

where ν denotes the number of degrees of freedom, $\delta\phi = 0.2°$ and $\delta m = 0.005$ being the experimental uncertainties in the measured phase and modulation values.

Estimation of the uncertainties in the recovered parameters is a difficult problem. We used the method described by Johnson and co-workers [22,23], which accounts for correlation between the parameters by a directed search of the χ_R^2 surface along directions predicted to display the highest degrees of correlation.

2.3. Multiexponential donor decays

For proteins in general [24] and melittin in particular [25], the intensity decays in the absence of energy transfer are heterogeneous and/or multiexponential. Hence, the formalism described above (eqs 1–17) must be modified to account for the intrinsic complexity of the tryptophan donor decay. The donor decay may be more complex than a multiexponential, and can possibly be described in terms of lifetime distributions [25–28]. In the presence of collisional quenching (below) the decays can be still more complex, and contain terms with varying time dependence [29–31]. Irrespective of the complexity of the decay, it is always possible to fit the data to a sum of exponentials, which is adequate for our purpose of representing the intensity decay as a parameterized function. Hence, we fit the donor decays in the absence of acceptor using a sum of exponentials

$$I_D^Q(t) = \sum_i \alpha_{Di}^Q \exp\left[-t/\tau_{Di}^Q\right] \tag{20}$$

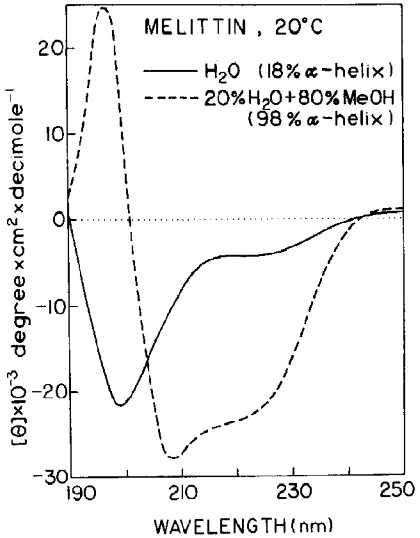

Fig. 1. CD spectra of melittin. Spectra are shown in water (———) and 80% methanol/20% water (- - - - -).

where α_{Di}^{Q} are the pre-exponential factors and τ_{Di}^{Q} the associated decay times. The superscript Q is an index for the quencher concentration (below), which was used to vary the Förster distance [11,12]. At the present time, we are unaware of an experimental demonstration of the precise rates of energy transfer for each component in a multiexponential decay. Also, such a determination may not be meaningful in those cases where the components originate with transient effects in quenching [29–31]. Consequently, we assumed that the

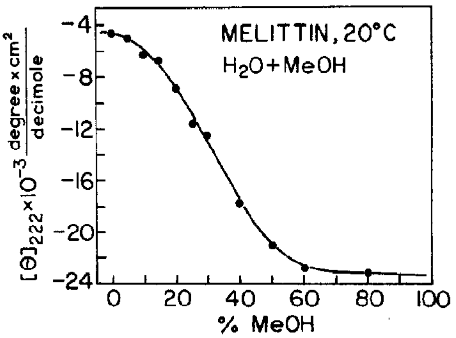

Fig. 2. Dependence of the ellipticity at 220 nm of melittin on the percentage of methanol.

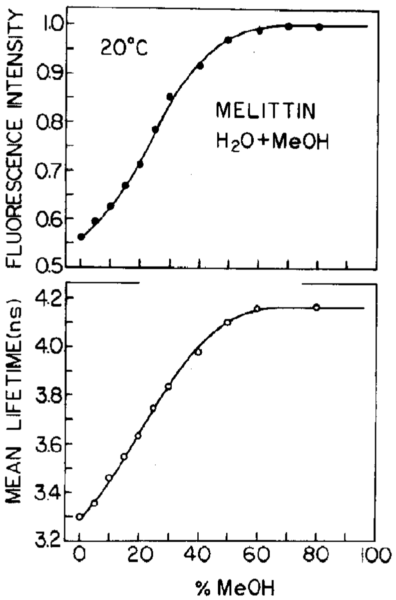

Fig. 3. Effect of methanol on the fluorescence intensity and mean lifetime of melittin tryptophan fluorescence.

Förster distance for transfer from each component in the donor decay is the same, and that the rates of transfer are the same relative to each decay

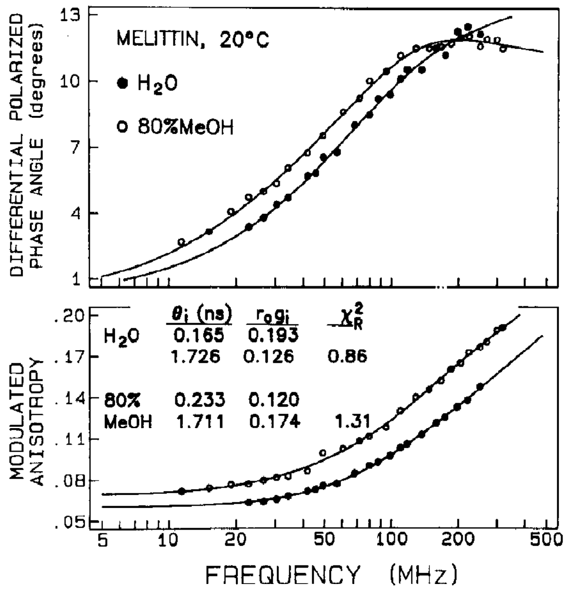

Fig. 4. Frequency-domain anisotropy decay of melittin in water (o) and 80% methanol/20% water (●). The intensity decays are given in table 1.

Table 1

Tryptophan and dansyl anisotropy decays for melittin and dansyl melittin

Compound/solvent	ϕ_i (ns)	$r_0 g_i$	χ^2_R	
			1[a]	2
Tryptophan emission				
Melittin/water	0.17	0.193	14.1	0.9
	1.73	0.126		
Dansyl-melittin/water	0.20	0.190		
	1.78	0.112	10.0	0.9
Melittin/80% MeOH	0.23	0.120		
	1.77	0.174	25.0	1.3
Dansyl-melittin/80% MeOH	0.25	0.122		
	1.80	0.174	12.6	1.2
Dansyl emission				
Dansyl-melittin/water	0.19	0.192	8.3	1.6
	1.87	0.114		
Dansyl-melittin/80% MeOH	0.28	0.165	3.3	1.0
	2.18	0.135		

[a] Values of χ^2_R are shown for the one- (1) and the two- (2) correlation-time fits. The anisotropy decay parameters are only shown for the accepted two-correlation-time model.

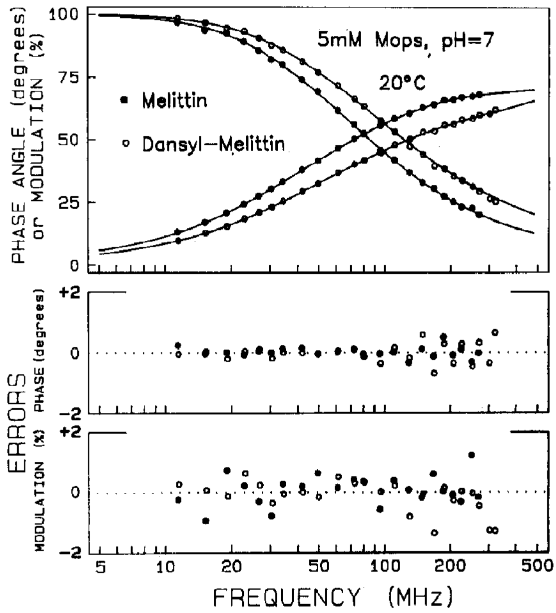

Fig. 6. Frequency response of the melittin tryptophan intensity decays in the absence (●) and presence (○) of the dansyl acceptor. The solid lines show the best triple-exponential fits to the data. 5 mM Mops, pH 7.

time. Hence, the transfer rates were assumed to be given by

$$k^{Q}_{DAi} = \frac{1}{\tau^{Q}_{Di}}\left(\frac{R^{Q}_{0}}{r}\right)^{6} \tag{21}$$

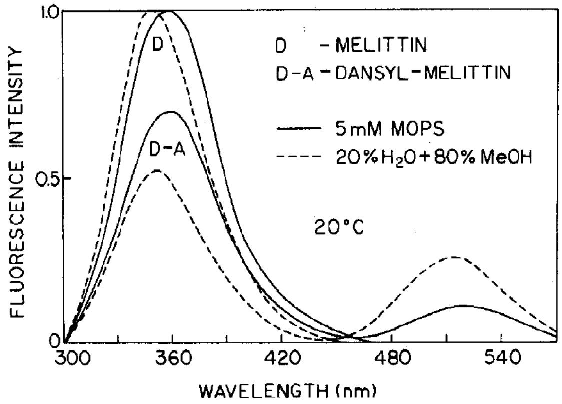

Fig. 5. Fluorescence emission spectra of melittin (D) and dansyl-melittin (D-A), in water (———) and 80% methanol/20% water (- - - - - -). Excitation at 290 nm.

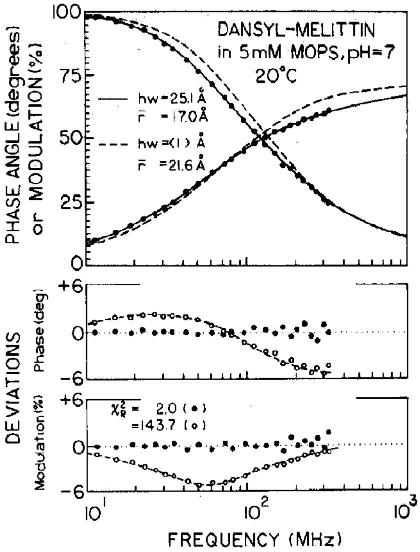

Fig. 7. Distance distribution analysis of the frequency response of dansyl-melittin in 5 mM Mops, pH 7. The solid line shows the best fit to the data (●). The dashed line shows the best fit with the hw held constant at 1 Å. The lower panels show the deviations with hw = 25.1 Å (●) and hw = ⟨1⟩ Å (○).

Table 2

Representative multiexponential analysis of the tryptophan intensity decays of melittin (5 mM Mops, pH 7, 20° C)

% MeOH	$\bar{\tau}$ (ns) [b]	τ_i (ns)	α_i	f_i	χ^2_R		
					1	2	3 [a]
0	3.29	0.32	0.408	0.065			
		2.49	0.401	0.495			
		4.64	0.191	0.400	548	5.7	1.4
10	3.45	0.33	0.393	0.060			
		2.82	0.460	0.595			
		5.11	0.147	0.345	504	5.9	2.3
20	3.62	0.42	0.365	0.062			
		2.98	0.342	0.412			
		4.45	0.293	0.526	438	2.1	1.3
30	3.77	0.43	0.333	0.056			
		3.04	0.526	0.626			
		5.82	0.141	0.318	402	6.0	1.6
40	3.96	0.52	0.352	0.069			
		3.19	0.516	0.620			
		6.25	0.132	0.310	462	6.5	2.2
60	4.18	0.67	0.374	0.092			
		2.97	0.437	0.474			
		6.30	0.189	0.434	546	7.2	2.2
80	4.19	0.67	0.375	0.092			
		2.96	0.434	0.468			
		6.29	0.192	0.440	551	7.7	2.8
0+6 M	4.67	0.65	0.257	0.063			
Gdn·HCl		3.14	0.698	0.831			
		6.18	0.045	0.106	151	2.1	1.4

[a] Values of χ^2_R are given for the single- (1), double- (2), and triple- (3) -exponential fits. The decay parameters are listed only for the triple-exponential fit.

[b] $\bar{\tau} = \sum f_i \tau_i = f_1\tau_1 + f_2\tau_2 + f_3\tau_3$.

The distance-dependent donor decay times are then expressed as

$$\frac{1}{\tau^Q_{DAi}} = \frac{1}{\tau^Q_{Di}} + \frac{1}{\tau^Q_{Di}}\left(\frac{R^Q_0}{r}\right)^6 \tag{22}$$

where R^Q_0 is the Förster distance appropriate for a given concentration of quencher (below). For an individual D-A pair the observed decay is given by

$$I^Q_{DA}(t) = \int_0^\infty \sum_i \alpha^Q_{Di} \exp\left[-\frac{t}{\tau^Q_{Di}} - \frac{t}{\tau^Q_{Di}}\left(\frac{R^Q_0}{r}\right)^6\right] dr. \tag{23}$$

The sine and cosine transforms are

$$N^Q_\omega = \int_0^\infty \sum_i \frac{P(r)\alpha_{Di}\omega\left(\tau^Q_{DAi}\right)^2}{1+\omega^2\left(\tau^Q_{DAi}\right)^2} dr \tag{24}$$

$$D^Q_\omega = \int_0^\infty \sum_i \frac{P(r)\alpha_{Di}\tau^Q_{DAi}}{1+\omega^2\left(\tau^Q_{DAi}\right)^2} dr \tag{25}$$

It should be noted that a multiexponential decay for the donor does not introduce any additional parameters into the analysis. This is because the intrinsic decays of the donor are measured in a separate experiment, using samples without an acceptor. The data from the donor are fitted using the multiexponential model, and the parameters (α_{Di}^{Q} and τ_{Di}^{Q}) are held constant in eqs. 24 and 25 during the least-squares analysis. It should be remembered that τ_{DAi}^{Q} depends on distance (eq. 22).

The uncertainties in $\bar{r}$ and hw were evaluated by the method proposed by Johnson [22,23], which accounts for correlation between the parameters. The uncertainty values were somewhat variable among the data sets, and probably not useful on a case-by-case basis. The average ranges of $\bar{r}$ and hw values consistent with the data were ± 0.2 and ± 0.4 Å, respectively.

2.4. Dependence of the Förster distance on collisional quenching

The ability to recover a distance distribution depends upon the value of R_0, which defines a range of distances over which the transfer is significantly dependent upon distance. We expanded the detectable range of distances using collisional quenching of the donor, which decreases the quantum yield and thereby decreases R_0 (eq. 5). We previously demonstrated that the appropriate quantum yields are given by the dynamic or collisional component in the quenching [11,12]. Hence,

Table 3

Representative multiexponential analyses of the tryptophan intensity decays of dansyl-melittin (5 mM Mops, pH 7, 20 °C)

% MeOH	$\bar{\tau}$ (ns) [b]	τ_i (ns)	α_i	f_i	χ_R^2 [a]		
					1	2	3
0	2.62	0.14	0.500	0.064			
		1.12	0.287	0.297			
		3.24	0.213	0.639	733	7.4	2.5
10	2.77	0.25	0.508	0.107			
		1.37	0.286	0.326			
		3.31	0.206	0.567	912	10.2	2.1
20	2.87	0.29	0.506	0.117			
		1.54	0.320	0.392			
		3.55	0.174	0.491	866	10.2	2.3
30	2.71	0.20	0.426	0.069			
		1.13	0.328	0.300			
		3.18	0.246	0.631	740	12.8	3.0
40	3.04	0.31	0.430	0.094			
		1.52	0.399	0.431			
		3.91	0.171	0.475	716	13.4	2.0
60	3.08	0.45	0.427	0.123			
		2.06	0.513	0.673			
		5.33	0.060	0.204	470	9.3	2.6
80	2.96	0.37	0.345	0.083			
		1.73	0.561	0.631			
		4.69	0.094	0.286	368	9.5	1.2
0+6 M	3.07	0.43	0.425	0.111			
Gdn·HCl		1.99	0.416	0.506			
		3.88	0.159	0.380	466	4.0	1.7

[a] Values of χ_R^2 are given for the single- (1), double- (2), and triple- (3) -exponential fits. The decay parameters are listed only for the triple-exponential fit.

[b] $\bar{\tau} = \sum f_i\tau_i = f_1\tau_1 + f_2\tau_2 + f_3\tau_3$.

Table 4

Distance-distribution parameters for dansyl-melittin in methanol/water mixtures

% MeOH	R_0 (Å)	$\bar{r}$ (Å)	hw (Å)	χ^2_R		
				F [a]	⟨1⟩	⟨25⟩ Å
0	19.9	17.0	25.1	2.0	143.7	2.0
10	21.5	18.0	23.3	1.8	182.1	1.9
20	21.9	18.4	20.6	2.1	210.5	3.84
30	22.3	20.9	16.6	3.1	139.8	12.4
40	23.0	22.8	14.6	2.0	93.3	12.5
50	23.3	24.1	9.0	3.5	29.2	58.8
60	23.5	24.5	4.6	3.0	4.7	101.9
80	23.6	25.0	3.0	2.1	2.3	93.6
0+6 M Gdn·HCl	19.9	16.6	30.4	1.4	129.7	2.0

[a] The values of χ^2_R are those found with the hw as a floating parameter (F) and with hw held fixed at ⟨1⟩ or ⟨25⟩ Å.

the appropriate quantum yields are given by

$$\phi_D^Q = \frac{\phi_D^0}{1 + K_D[Q]} \tag{26}$$

where ϕ_D^0 is the quantum yield in the absence of quenching, K_D the dynamic quenching constant and [Q] concentration of quencher. The quenching-dependent Förster distances are then given by

$$R_0^Q = R_0 \left(\frac{\phi_D^Q}{\phi_D^0} \right)^{1/6}. \tag{27}$$

Data measured at a single value of R_0^Q can be analyzed using eqs. 21–26 with the appropriate value of R_0^Q. These analyses reveal whether $P(r)$ depends upon the distance window. Alternatively, the data at several R_0^Q values (quencher concentrations) may be analyzed simultaneously (globally) to recover a single distance distribution. In this case the sum in eq. 19 extends over both the frequencies (ω) and the quencher concentrations [Q].

2.5. Anisotropy decays

Anisotropy decays were obtained from the frequency-domain data, as described previously [6,7]. The measured values are the phase angle difference between the polarized components of the emission and the modulated anisotropies. These data are fitted to the multiexponential decay law:

$$r(t) = \sum_i r_0 g_i e^{-t/\theta_i} \tag{28}$$

where $r_0 g_i$ are the amplitudes of the anisotropy decay associated with each correlation time (θ_i).

3. Materials and methods

Melittin was prepared by total synthesis using standard solid-phase procedures with an Applied Biosystems peptide synthesizer [32]. Dansyl melittin was prepared from the synthetic melittin by chemically reacting dansyl chloride with the deblocked NH_2 of the amino-terminal glycine residue, washing of the resin to eliminate residual dansyl chloride, and finally cleavage of the peptide from the resin and complete deblocking with HF. All peptides were purified by reverse-phase HPLC on a C_{18} column and eluted with a water/acetonitrile gradient. Purity of the peptides was determined from fast-atom bombardment mass spectrometry (FAB/MS) by Dr. Ian Jardine, Department of Pharmacology, Mayo Foundation. To obtain the random-coil state, melittin and/or dansyl-melittin was dissolved in 5 mM Mops (pH 7). At these low ionic strengths, melittin is known to be monomeric [33,34]. The α-helical state was induced using methanol/water mixtures ranging up to 80% methanol (v/v). Under these conditions, melittin is known to adopt an α-helical conformation, but to remain in the monomeric state [32,35]. We measured the extent of random-coil–α-helix in these mixtures by CD using an Aviv spectrophotometer. The percentage of each conformation was determined using a nonlinear least squares procedure, according to the basis spectra described by Chen et al. or by Greenfield and Fasman [36,37].

Fluorescence emission spectra were recorded on all samples and blanks, and were found to indicate the absence of signals due to impurities in the solvent. Quantum yields of the donor were measured relative to a value of 0.13 for tryptophan in water at 20 °C [38].

Frequency-domain measurements were performed using the instrument described previously in detail [7]. The excitation source was a 3.79 MHz train of pulses, about 7 ps wide, obtained from the cavity-dumped output of a synchronously pumped rhodamine 6G dye laser. The rhodamine 6G and

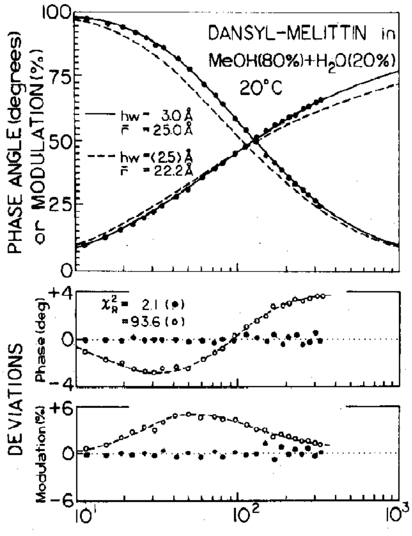

Fig. 8. Distance distribution analysis of the frequency response of dansyl-melittin in 80% methanol/20% water. The solid line shows the best fit to the data (●). The dashed line shows the best fit with the hw held constant at 25 Å. The lower panels show the deviations with hw = 3 Å (●) and hw = ⟨25⟩ Å (○).

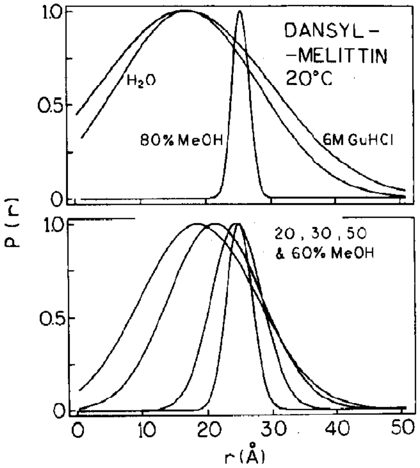

Fig. 9. (Top) Distance distributions of dansyl melittin in H_2O (5 mM Mops), 6 M Gdn·HCl and 80% methanol/20% water. (Bottom) Distance distributions in methanol/water mixtures.

pyridine 2 dye lasers were frequency-doubled to 290–300 and 350–370 nm for excitation of the tryptophan and dansyl residues, respectively. These sources are intrinsically modulated to several gigahertz, and are used directly to excite the sample. The modulated emission was detected using a microchannel plate photomultiplier tube (R1564U, Hamamatsu Corp.), which was externally cross-correlated. All intensity decays were measured using rotation-free polarization conditions. The donor emissions were selected using an interference filter with a 10 nm bandpass, centered at 360 nm. The data are initially transferred to a dedicated Minc 11/23 for storage, then to a Dec 11/73 for analysis [39,40]. For all analyses the estimated uncertainties were 0.2° in the phase angle and 0.005 in the modulation.

4. Results

4.1. Effects of methanol on the conformation of melittin

Prior to measuring the distance distributions of melittin, we examined the effects of methanol/water mixtures on its intrinsic spectroscopic properties. CD spectra in water (———) and 80%

methanol/water (- - - - - -) are shown in fig. 1. The CD spectrum in 80% methanol is characteristic of an α-helix [36], and in fact predicts 98% α-helix under these conditions. This spectrum is similar to that observed for melittin in water at high salt concentrations [38], a solvent condition which is also known to induce α-helix formation. However, the extent of helix formation is apparently not as high for melittin in solution of high ionic strength as for the peptide in methanol/water mixtures with a high mole fraction of methanol [35]. The CD spectrum in water (5 mM Mops) is predominantly that of a random-coil peptide with a small amount of α-helix, i.e., approx. 18%. This is consistent with previous NMR data which suggest some residual structure in the monomeric state of melittin in water [41].

We used the negative band at 222 nm to follow the progressive effects of methanol on the conformation of melittin (fig. 2). These data suggest that the random-coil to α-helix transition is 50% complete at 30% methanol, and is essentially complete at 60% methanol. This transition was corroborated by measurements of the fluorescence intensity and mean decay time (fig. 3) which also indicated midpoints and endpoints of 30 and 60% methanol, respectively. We also examined the frequency-domain anisotropy decays of the intrinsic tryptophan emission of melittin (fig. 4). At both extremes of solvent composition (0 and 80% methanol), the anisotropy decay contains a correlation time near 1.7 ns (table 1), which is characteristic of monomeric melittin [42]. Similar correlation times were obtained using the dansyl emission from dansyl-melittin. If tetrameric melittin were present then one would expect a longer correlation time near 3.4 ns. It is interesting to note that the extent of segmental mobility displayed by the tryptophan residue is larger in the random-coil state (H_2O) than in the α-helical form (80% methanol), as would have been predicted from first principles. In the random-coil state the subnanosecond correlation time accounts for 61% of the total anisotropy decay, whereas in the α-helical state this component contributes 41% of the anisotropy decay. It should also be noted that the short correlation time recovered in this experiment for melittin in water is somewhat longer than that reported previously [42]. This is not a discrepancy, but rather reflects the lower time resolution of the present anisotropy measurements, which were not performed in the presence of collisional quenching in order to obtain maximal resolution of the rapid motions. We also examined the tryptophan anisotropy decays of dansyl-melittin. These anisotropy decay parameters (table 1) are essentially identical to that found for unlabeled melittin, suggesting that the dansyl label does not interfere with the random-coil to α-helical transition. In summary, the data in figs 1–4 demonstrate that melittin undergoes a random-coil to α-helix transition in the methanol/water mixtures, remains in the monomeric state in methanol, and that the conformational transition is not perturbed by the dansyl label.

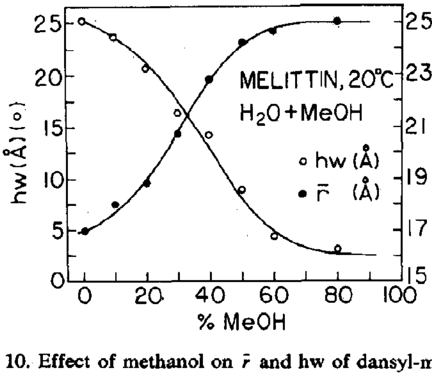

Fig. 10. Effect of methanol on $\bar{r}$ and hw of dansyl-mellitin.

4.2. Emission spectra of melittin and dansyl-melittin

Emission spectra of melittin and dansyl melittin are shown in fig. 4. For easier comparison we normalized the peak intensities of the unlabeled sample (D) to the same peak value. The presence of the dansyl acceptor results in about 30% energy transfer in water, which increases to 53% in 80% methanol. The increase in energy transfer in 80% methanol is evident from both the decrease in donor intensity and an increase in acceptor intensity. These data can be used to calculate an apparent distance (r_{app}) from the tryptophan residue to the dansyl group using

$$r_{app} = R_0\left(\frac{1-E}{E}\right)^{1/6} \tag{29}$$

where E is the efficiency of energy transfer. Using the R_0 values appropriate for these conditions, the apparent distances are 22.9 and 24.1 Å in water and 80% methanol, respectively. However, it should be emphasized that these apparent values only have physical significance if there exists a single distance between the donor and the acceptor.

4.3. Frequency-domain tryptophan decays

To obtain more detailed information on the donor-to-acceptor distance distributions we examined the donor intensity decays using the frequency-domain method. Representative data for unlabeled (●) and labeled (○) melittin are shown in fig. 6. The presence of the dansyl acceptor results in a shift in the tryptophan frequency response to higher frequencies, which is the result of its shortened lifetime due to energy transfer. In both cases the data can be fitted using the triple-exponential model, as can be seen from the overlap of the data (●, ○) with the calculated frequency responses (———) and from the small and random deviation between the data and the calculated phase and modulation values (fig. 6, lower panels).

For all melittin samples, with and without acceptor and at all methanol concentrations, it was necessary to use the triple-exponential model to account for the data. This is seen from the large values of χ_R^2 obtained from the single-exponential fits (tables 2 and 3), which range from 150 to 900. Even the double-experimental model is inadequate, since the value of χ_R^2 decreased 1.6–7-fold for the triple-exponential fits. In the case of unlabeled melittin the intensity decay parameters are characteristic of the native protein. It is interesting to note that the tryptophan decay of melittin appears to be closest to a single exponential when the peptide is dissolved in 6 M Gdn · HCl. This result is consistent with our previous suggestion that conformational heterogeneity is one cause of decay time heterogeneity in proteins [43].

Tables 2 and 3 summarize representative intensity decays for melittin and dansyl-melittin, respectively. In the present paper the frequency response of the emission was used to recover the distance distributions. However, we cannot be certain that our assumed Gaussian model (eq. 8) is unique or correct. The parameterized decays in tables 2 and 3 provide one basis for comparing the present frequency-domain results with future time-domain measurements on the same system or model calculations of the distance distribution based on assumed rotational potential energy functions for the melittin peptide. It should also be borne in mind that the intensity decays of melittin contain different types of information in the absence and presence of the dansyl acceptor. In the absence of acceptor (table 2) the decays are determined by the structure and dynamics of native melittin. In the presence of acceptor (table 3) these same factors are present, with additional complexity induced by the distant-dependent energy transfer from tryptophan to dansyl.

4.4. Distance distribution analysis of dansyl-melittin

The intensity decays of dansyl-melittin could be analyzed in several ways, including the multiexponential (tables 1 and 2, refs 6 and 20) and lifetime distribution models [25–28]. However, parameters contained in these models do not reflect the molecular feature of interest, which is the distribution of tryptophan to dansyl distances. Hence, the intensity decays were analyzed in a pairwise manner (D vs D-A pair) to recover the mean ($\bar{r}$) and half-width (hw) of the distance distribution (eq. 8). In this analysis the parameters (α_i and τ_i) which describe the intensity decay (table 2) are held constant in the fitting procedure. The values of $\bar{r}$ and hw are varied to obtain the best fit to the frequency response of the D-A pair. A representative case is shown in fig. 7 for dansyl-melittin in water. The data (●) are in agreement with the frequency response predicted for $\bar{r} = 17$ Å and hw = 21.6 Å, as can be seen from the overlap of the calculated curve (———) with the data (●, top panel), the small and random deviations (lower panels), and the acceptable value of χ_R^2. In this case the data indicate that there exists a wide distribution of tryptophan to dansyl distances.

We questioned whether the data could be accounted for by an acceptor located at a single distance. Hence, the analysis was repeated with

Table 5

Representative intensity decays of melittin and dansyl-melittin tryptophan fluorescence with 0.4 M acrylamide

% MeOH	$\bar{\tau}$ (ns)	τ_i	α_i	f_i	χ_R^2		
					1	2	3
Melittin							
0		0.09	0.598	0.155			
		0.66	0.384	0.718			
	0.79	2.43	0.018	0.127	478	14.8	1.7
30		0.10	0.374	0.054			
		0.87	0.434	0.531			
	1.10	1.54	0.192	0.414	206	3.7	1.5
80		0.15	0.442	0.103			
		0.98	0.542	0.829			
	1.01	2.65	0.017	0.068	280	3.7	1.9
Dansyl-melittin							
0		0.09	0.663	0.212			
		0.55	0.316	0.647			
	0.63	1.81	0.021	0.141	736	13.7	2.3
30		0.11	0.435	0.092			
		0.62	0.404	0.497			
	0.84	1.28	0.161	0.411	385	6.0	1.1
80		0.11	0.422	0.093			
		0.73	0.527	0.755			
	0.80	1.53	0.051	0.152	253	4.1	1.9

the hw held constant at 1 Å while $\bar{r}$ was permitted to vary to minimize χ_R^2. In this case, the calculated curve (- - - - - -) did not overlap with the data (●), the deviations being large and systematic (o, lower panels), and the value of $\chi_R^2 = 143.7$ unacceptable. This result demonstrates that there is increased heterogeneity in the donor decay due to energy transfer, which we believe is due to a distribution of D to A distances.

A similar analysis is presented in fig. 8, except for the use of 80% methanol as the solvent. In this case melittin is expected to be in the α-helical state. The frequency response is now consistent with a narrow distribution of tryptophan to dansyl distances, viz., hw = 3 Å. We attempted to fit the data to a wide distribution of distances ($\bar{r}$ = 25 Å) but this resulted in an unacceptable fit (- - - - - -) and an elevated value of $\chi_R^2 = 93.6$. Hence, the data for dansyl-melittin in methanol are not consistent with a wide distribution of distances.

The distance distributions in water and 80% methanol are shown schematically in fig. 9. There is already a dramatic shift towards a single distance in the presence of 80% methanol. We were encouraged by these results and addressed the question of whether we could detect a progressive shift in conformation at various concentrations of methanol.

As the concentration of methanol is increased the distance distribution shifts progressively towards that of the α-helical state (fig. 9, bottom). The average distance $\bar{r}$ increases from 17 to 25 Å, and the hw decreases dramatically from 25 to 3 Å (fig. 10 and table 4). This transition is evident from attempts to fit the data using fixed half-widths of 1 or 25 Å (table 4). The values of χ_R^2 for a constant hw = ⟨1 Å⟩ decrease progressively with increasing concentrations of methanol, and the values of χ_R^2 for a constant hw = ⟨25 Å⟩ increase progressively. Our ability to detect this progressive conformational change (fig. 10) illustrates the reliability of the recovered distribution and the general usefulness of this method for studies of conformational changes and/or folding pathways for proteins. Interestingly, a still wider distribution was observed in 6 M Gdn · HCl (fig. 9, top; and table 4), indicating the disruption of residual structure by this denaturant.

4.5. Variation of the Förster distance by quenching

In any energy-transfer experiment the measurable range of distances is limited by the Förster distance for transfer. In previous publications we described the use of collisional quenching to decrease the quantum yield of the donor and thereby decrease R_0 [11,12]. We used acrylamide quenching [44] of the tryptophan emission to vary R_0 for transfer to the dansyl acceptor. The intensity decays of melittin and dansyl-melittin are summarized in table 5. It should be recalled that such quenching induces increased heterogeneity in the decay, but that this heterogeneity is accounted for by our fitting algorithm.

The distance distributions at each R_0^Q value (each acrylamide concentration) are summarized in table 6 and fig. 11. The values of $\bar{r}$ and hw are not dependent upon the value of R_0^Q, at least over the limited range accessible by quenching. Also, the data at all three acrylamide concentrations are equally well fitted by a global analysis as by the individual analyses. These results suggest that the

Table 6

Distance-distribution parameters of dansyl-melittin obtained with various Förster distances

% MeOH	[Acrylamide] (M)	R_0 (Å)	$\bar{r}$ (Å)	hw (Å)	χ_R^2
0	0	19.9	17.0	25.1	2.0
	0.2	17.6	18.4	27.4	2.8
	0.4	16.6	18.3	23.6	2.4
	0–0.4	–	18.1	24.4	4.3
30	0	22.3	20.9	16.6	3.1
	0.2	20.2	21.2	16.7	1.4
	0.4	19.1	21.8	15.6	1.3
	0–0.4	–	21.4	15.9	2.3
80	0	23.6	25.0	3.0	2.1
	0.2	20.8	24.7	3.6	2.6
	0.4	19.8	24.9	0.1	2.1
	0–0.4	–	24.7	2.3	4.8

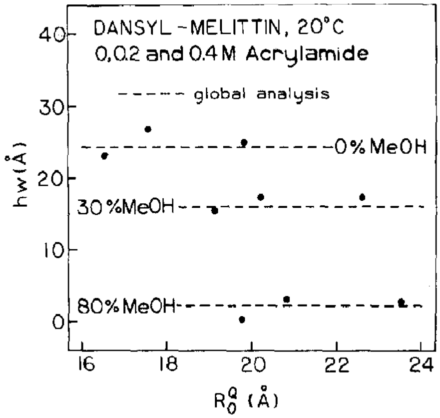

Fig. 11. Evaluation of $\bar{r}$ and hw with different Förster distances for energy transfer.

distribution model is adequate for the present data. Attempts to fit the data to a more complex skewed Gaussian did not result in a significant decrease in χ_R^2 (not shown).

5. Discussion

What is the physical origin of the distribution of distances observed for tryptophan to dansyl energy transfer? We believe that the dominant factor is the flexibility of the peptide, with other effects being less significant. The latter effects include lack of resolution, local mobility of the donor and acceptor moieties, effects of the orientation factor κ^2 on the rate of transfer, and Trp-to-dansyl diffusive motions of the peptide chain. The fact that we observed an hw of only 3 Å in 80% methanol suggests our data are probably adequate to resolve a distribution as narrow as 3 Å. Hence, lack of resolution is unlikely to be the origin of the wide distributions observed for melittin at low ionic strength. Also, the tryptophan side chain and dansyl moiety are not directly involved in the α-helical structure, so their local mobility is likely to be similar in the putative random-coil and α-helical states. Hence, these factors (resolution and local motion freedom) are unlikely to contribute more than 3 Å to the width of the distribution.

The effects of κ^2 on the measured distances and distance distribution have been the subject of considerable controversy [18,19]. The formalism developed by Dale et al. [18] probably represents the maximum uncertainty in the distance due to the unknown value of κ^2. This theory assumes the absorption and emission is due to single transition moments. According to Dale et al., the maximum and minimum values of κ^2 can be calculated from the depolarization of the donor and acceptor which is due to segmental motion of these residues,

$$\kappa^2_{\min} = \tfrac{2}{3}\left[1 - \left(d^x_D + d^x_A\right)/2\right] \quad (30)$$

$$\kappa^2_{\max} = \tfrac{2}{3}\left[1 + d^x_D + d^x_A + 3 d^x_D d^x_A\right] \quad (31)$$

where

$$d^x_i = \left(r_i/r_0\right)^{1/2} \quad (32)$$

The value of r_i should represent the fractional depolarization due to segmental motion of the residue (d_i), but not the depolarization due to overall rotational diffusion of the protein (d_p). These values are related to the steady-state anisotropy (r) by

$$r = r_0 d_i d_p \quad (33)$$

where

$$d_p^{-1} = 1 + \tau/\theta_p \quad (34)$$

and τ designates the decay time of the probe and θ_p the rotational correlation time of the protein [47]. The theory of Dale et al. [18] assumes single transition moments, which implies the use of $r_0 =$ 0.4 for both the donor and acceptor. However, we chose the more conservative approach of using the values of r_0 recovered from the anisotropy decay measurements (fig. 4). We assumed that the dansyl residue displayed similar local mobility to that of the tryptophan residue. These assumptions result in depolarization factors of $\langle d^x_D \rangle = \langle d^x_A \rangle = 0.78$ and 0.64 for random-coil and α-helical melittin, respectively. These values lead to lower and upper limits of κ^2 of 0.15 and 2.92, respectively (eqs 30–32). These values of κ^2 indicate that the distances can range from 0.75 to 1.29 of the apparent distance ($\bar{r}$). For instance, for the average distance of 17 Å found for α-helical melittin, the distances could range from 13.2 to 21.9 Å, which is a width of nearly 9 Å. However, the distribution recovered for α-helical melittin was only 3 Å wide, which suggests that in reality κ^2 contributes no more than this amount to the widths of the distribution.

The accuracy of the procedures just described was particularly well demonstrated in this work because of the unique conformational tendencies of melittin. We used molecular graphics to measure the distance of the amino moiety at the N-terminal to the indole ring and found this to be 24 Å, in excellent agreement with the value of 25 Å determined from the fluorescence resonance energy transfer measurements. The very small difference is probably fortuitous and in any event is quite insignificant. Nevertheless, differences between measured and estimated distances in melittin might reflect: (i) the error inherent in the method; (ii) the fact that the crystal structure is that of tetrameric melittin [13] in which each melittin monomer is apparently less helical and less extended than melittin in methanol-water mixtures [35]; and (iii) that the distance measured by FRET is from the dansyl moiety not from the amino group to the tryptophan side chain.

For a fully extended melittin monomer, the distance from the amino terminal to that Trp side chain could be in excess of 54 Å. Interestingly, this is the approximately maximal distance suggested by the distribution analysis of the FRET data for the assumed random-coil form of the melittin monomer. However, the data on this form of the peptide also raise some interesting questions regarding this putatively 'random' form of melittin in water. First, it is apparent from the effects of Gdn · HCl that melittin retains a small amount of residual (α-helix) structure at low ionic strength, an inference in keeping with the results from CD measurements [45]. Second, the width of the apparent distribution suggests a large number of conformational substates for the peptide in water but the data do not allow us to distinguish between a static and dynamic distribution of substates. A priori, given the viscous drag imposed by the solvent, and the short decay time of the tryptophan donor near 3 ns, it seems improbable that the conformational substates would all interconvert on a nanosecond time scale. Admittedly, the time-resolved anisotropy data have shown clearly that the indole moiety has mobility on the picosecond time scale [42]. This inference is corroborated strongly by recent ^{13}C-NMR relaxation data [46]. In addition, the amino- and carboxy-terminal residues are expected to exhibit nanosecond mobility even for the helical peptide ('end effects'). Thus, the broad distribution most likely reflects a complex mixture of static and dynamic (interconverting) conformations. Third, the significance of the position of the apparent center of the distribution for the random form of the peptide is not clear. The proline moiety at position 14 of the sequence could conceivably so influence the conformation as to invalidate the assumption of a Gaussian distribution in which case the value of 18 Å obtained here for the center of the distributed states would have less physical significance. Nonetheless, it is of interest to compare the distance distribution recovered from these experiments with that predicted from theory based on the putatively known rotational potential functions for the amino acids in the peptide chain.

Acknowledgements

This work was supported by Grant GM 35154 from the National Institutes of Health, with support for instrumentation from the National Science Foundation (DMB 8502835 and 8511065) to J.R.L., by Grant GM 34847 from the National Institutes of Health to F.G.P., and from the Center for Fluorescence Spectroscopy at the University of Maryland. The authors thank Mr. Paul Yadlowsky, University of Virginia, for assistance with measuring distances from the crystal structure. J.R.L. and G.L. wish to acknowledge support from the Medical Biotechnology Center, University of Maryland.

References

1 L. Stryer, Annu. Rev. Biochem. 47 (1978) 819.
2 I.Z. Steinberg, Annu. Rev. Biochem. 40 (1971) 83.
3 J.R. Lakowicz, Principles of fluorescence spectroscopy (Plenum, New York, 1983) ch. 10, p. 303.
4 T. Förster, Ann. Phys. (Leipzig) 2 (1948) 55.
5 E. Gratton and M. Limkeman, Biophys. J. 44 (1983) 315.
6 J.R. Lakowicz and B.P. Maliwal, Biophys. Chem. 21 (1985) 61.
7 J.R. Lakowicz, G. Laczko and I. Gryczynski, Rev. Sci. Instrum. 57 (1986) 2499.
8 J.R. Lakowicz, M.L. Johnson, W. Wiczk, A. Bhat and R.F. Steiner, Chem. Phys. Lett. 138 (1987) 587.
9 J.R. Lakowicz, I. Gryczynski, H.C. Cheung, C.K. Wang and M.L. Johnson, Biopolymers 27 (1988) 821.
10 J.R. Lakowicz, I. Gryczynski, H.C. Cheung, C.K. Wang, M.L. Johnson and N. Joshi, Biochemistry 27 (1988) 9149.
11 I. Gryczynski, W. Wiczk, M.L. Johnson and J.R. Lakowicz, Chem. Phys. Lett. 145 (1988) 437.
12 I. Gryczynski, W. Wiczk, M.L. Johnson, H.C. Cheung, C.K. Wang and J.R. Lakowicz, Biophys. J. 54 (1988) 577.
13 T.C. Terwilliger and D. Eisenberg, J. Biol. Chem. 257 (1982) 6016.
14 E. Haas, H. Wilchek, E. Katchalski-Katzir and I.Z. Steinberg, Proc. Natl. Acad. Sci. U.S.A. 72 (1975) 1807.
15 D. Amir and E. Haas, Biopolymers 25 (1986) 235.
16 E. Haas, E. Katchalski-Katzir and I.Z. Steinberg, Biopolymers 17 (1978) 11.
17 E. Katchalski-Katzir and I.Z. Steinberg, Ann. N.Y. Acad. Sci. 366 (1981) 41.
18 R.E. Dale, J. Eisinger and W.E. Blumberg, Biophys. J. 26 (1979) 161.
19 E. Haas, E. Katchalski-Katzir and I.Z. Steinberg, Biochemistry 17 (1978) 5064.
20 J.R. Lakowicz, E. Gratton, G. Laczko, H. Cherek and M. Limkeman, Biophys. J. 46 (1984) 463.
21 P.R. Bevington, Data reduction and error analysis for physical sciences (McGraw-Hill, New York, 1969).
22 M.L. Johnson, Biophys. J. 44 (1983) 101.
23 M.L. Johnson and S.G. Frasier, Methods Enzymol. 117 (1985) 301.
24 J.M. Beechem and L. Brand, Annu. Rev. Biochem. 54 (1985) 43.
25 J.R. Acala, E. Gratton and F.G. Prendergast, Biophys. J. 51 (1987) 587.
26 J.R. Acala, E. Gratton and F.G. Prendergast, Biophys. J. 51 (1987) 597.
27 J.R. Acala, E. Gratton and F.G. Prendergast, Biophys. J. 51 (1987) 925.
a D.R. James and W.R. Ware, Chem. Phys. Lett. 126 (1986) 7.
b D.R. James and W.R. Ware, Chem. Phys. Lett. 120 (1985) 455.
28 J.R. Lakowicz, H. Cherek, I. Gryczynski, N. Joshi and M.L. Johnson, Biophys. Chem. 28 (1987) 35.
29 N. Joshi, M.L. Johnson, I. Gryczynski and J.R. Lakowicz, Chem. Phys. Lett. 135 (1987) 200.
30 J.R. Lakowicz, M.L. Johnson, I. Gryczynski, N. Joshi and G. Laczko, J. Phys. Chem. 91 (1987) 3277.
31 J.R. Lakowicz, N.B. Joshi, M.L. Johnson, H. Szmacinski and I. Gryczynski, J. Biol. Chem. 262 (1987) 10907.
32 A.J. Weaver, M.D. Kemple and F.G. Prendergast, Biochemistry 28 (1989) 8624.

33 J.C. Talbot, J. Dufourcq, J. deBong, J.R. Faucon and C. Lurson, FEBS Lett. 102 (1979) 191.
34 J.F. Faucon, J. Dufourcq and C. Lurson, FEBS Lett. 102 (1979) 187.
35 R. Bazzo, M.J. Tappin, A. Pastore, T.S. Harvey, J.A. Carver and I.D. Campbell, Eur. J. Biochem. 173 (1988) 139.
36 Y.H. Chen, J.T. Yang and K.H. Chau, Biochemistry 13 (1974) 3350.
37 N. Greenfield and G.D. Fasman, Biochemistry 8 (1969) 4108.
a A.S. Tatham, R.C. Hider and A.F. Drake, Biochem. J. 211 (1983) 683.
38 R.F. Chen, Anal. Lett. 1 (1967) 35.
39 J.R. Lakowicz, E. Gratton, G. Laczko, H. Cherek and M. Limkeman, Biophys. J. 46 (1984) 463.
40 E. Gratton, J.R. Lakowicz, B. Maliwal, H. Cherek, G. Laczko and M. Limkeman, Biophys. J. 46 (1984) 479.
41 J. Jentsch, Z. Naturforsch. 24b (1969) 33.
42 J.R. Lakowicz, H. Cherek, I. Gryczynski, N. Joshi and M.L. Johnson, Biophys. J. 51 (1987) 755.
43 I. Gryczynski, M. Eftink and J.R. Lakowicz, Biochim. Biophys. Acta 954 (1988) 242.
44 M.R. Eftink and C.A. Ghiron, J. Phys. Chem. 80 (1976) 486.
45 R.A. Yunes, Arch. Biochem. Biophys. 216 (1982) 559.
46 A.J. Weaver, M.D. Kemple and F.G. Prendergast, Biochemistry 28 (1989) 8614.
47 J.R. Lakowicz and G. Weber, Biophys. J. 32 (1980) 591.